Electrochemistry Communications 10 (2008) 827–830

Contents lists available at ScienceDirect

Electrochemistry Communications

journal homepage: www.elsevier.com/locate/elecom

# Fabrication and characterization of gold nanoclusters on phosphorus incorporated tetrahedral amorphous carbon electrode

Aiping Liu *, Jiaqi Zhu, Jiecai Han, Huaping Wu, Chunzhu Jiang

*Center for Composite Materials, Harbin Institute of Technology, Postbox 3010, Yikuang Street 2, Nangang District, Harbin 150080, PR China*

ARTICLE INFO

*Article history:*
Received 1 March 2008
Received in revised form 13 March 2008
Accepted 17 March 2008
Available online 27 March 2008

*Keywords:*
Gold nanoclusters
Phosphorus incorporated tetrahedral amorphous carbon electrode
Electrodeposition
Electroanalysis

ABSTRACT

Gold nanoclusters (NCs) were electrodeposited on phosphorus incorporated tetrahedral amorphous carbon (ta-C:P) electrode and characterized by X-ray photoelectron spectroscopy, scanning electron microscopy, cyclic voltammetry and chronoamperometry. The nanosized Au deposits controlled by adjusting the deposition time represented a progressive nucleation and diffusion-controlled growth of separate three-dimensional islands on limited sites. Significant enhancement of electrochemical activity and reversibility towards ferricyanide oxidation reaction was observed after the deposition of Au NCs on ta-C:P film, implying ta-C:P/Au as a potential material for the application of electroanalysis.



## 1. Introduction

Great attention has been given to metal nanoparticles (NPs) due to their abilities to enhance catalytic activity of electrodes, facilitate electron transfer and improve sensitivity and selectivity of electrodes. Materials assembled with two- and three-dimensional NPs become important in analytical chemistry in terms of their potential applications in nanoelectronic devices, sensors and catalysts [1–3]. Gold NPs or nanoclusters (NCs) with a large surface area and a good electronic property show specific performances of accumulating charge, which makes them promising as preponderant materials in the construction of electrochemical sensors and biosensors [4–6]. Currently, many technologies have been adopted to prepare Au NPs/NCs including electrochemical deposition (a convenient, efficient and fast method) [6–8], metal vapor synthesis [9], ion-beam [10] and sputtering deposition [11], sol–gel technique [3–5], and so on. Many groups have investigated the properties of Au NPs/NCs on carbon-based materials, such as glassy carbon [12], screen-printed carbon [7], amorphous carbon (a-C) [10] and boron doped diamond (BDD) [6,9,11]. Among which, a-C electrodes are suggested to be an inexpensive, hence well alternative to crystalline diamond electrodes [13]. With ambient temperature growth on virtually any substrate and smooth surfaces, a-C films exhibit many important advantages over the difficult-to-nucleate, high-temperature grown polycrystalline BDD films [13], especially in the applications for water treatment and bioelectrodes [14,15]. With platinum, nitrogen or phosphorus used as a dopant, doped a-C electrodes are regarded as appropriate for the application in electroanalytical chemistry [14,16–19]. However, the electrocatalytic activity of the doped a-C electrodes is still limited. Metallic modification should be attempted to improve the electrochemical response of the electrodes.

In the present investigation, phosphorus incorporated tetrahedral amorphous carbon (ta-C:P) film is firstly prepared on silicon wafers by filtered cathodic vacuum arc (FCVA) technology, followed by an electrodeposition of Au NCs on the film surface. The resulted Au deposits are characterized by X-ray photoelectron spectroscopy (XPS), scanning electron microscopy (SEM), cyclic voltammetry and chronoamperometry. The electrochemical activity of Au NCs modified ta-C:P (ta-C:P/Au) electrodes towards ferricyanide oxidation reaction is examined in detail.

## 2. Experimental

70–80 nm ta-C and ta-C:P films were deposited on conductive Si wafers by FCVA system [19] with 8 sccm $PH_3$ gas as the dopant source. The electrochemical deposition of Au NCs on ta-C:P surface was performed in 0.1 M $H_3BO_4$ + $H_2SO_4$ solution containing 0.5 mM $HAuCl_4$ (pH 1.4) using an electrochemical workstation (CHI 660A, China). The three–electrode system consisted of ta-C:P working electrode, saturated calomel electrode (SCE) reference electrode and platinum counter electrode. The edges and backsides of ta-C:P were sealed by an O-ring resin with the apparent geometric surface area of 0.4 $cm^2$. The potential was scanned from 0.85 V to

* Corresponding author. Tel.: +86 451 86402954; fax: +86 451 86417970.
*E-mail address:* liuaiping1979@gmail.com (A. Liu).

1388-2481/$ - see front matter © 2008 Elsevier B.V. All rights reserved.
doi:10.1016/j.elecom.2008.03.012

−0.05 V (vs. SCE) and back to 0.85 V for different cycles at 0.02 $V s^{-1}$.

Compositions of ta-C:P film (P/(C+P) = 5.8 ± 0.2 at.%) was quantified by XPS signals recorded on a PHI ESCA 5700 spectrometer. Core level spectra of Au 4f and C 1s were analyzed as a function of depth by Argon ion sputtering at 3 keV. The morphology of Au NCs was examined using a Hitachi S4800 SEM. The deposition process and nucleation mechanism of Au were analyzed by cyclic voltammetry and chronoamperometry, respectively. The kinetics of $Fe(CN)_6^{3-/4-}$ redox couple was investigated in 5 mM $K_3Fe(CN)_6$ and 1 M KCl solution at 0.02 $V s^{-1}$.

## 3. Results and discussion

### 3.1. Voltammetric properties of Au electrodeposition

Fig. 1 displays cyclic voltammograms (CVs) of ta-C:P electrode in 0.5 mM $HAuCl_4$ solution at 0.02 $V s^{-1}$. The curve shape is similar to those reported in previous studies [20]. A reduction peak of Au (Peak A) is observed at about 0.16 V in the first scan. The peak at −0.30 V (Peak B) is related to the reduction of hydrogen ions to hydrogen adatoms [21]. The peak at 1.14 V (Peak C) on the returning curve is verified due to the oxidation of deposited Au on ta-C:P surface. A crossover of forward and reverse currents is observed at 0.81 V, corresponding to the equilibrium potential of $Au/Au^{3+}$ reaction. Peak A in the second cycle shifts to a more positive potential of 0.61 V. This can be explained by the suggestion that the existent Au nuclei make the deposition of Au easier. Peak B also moves towards more positive direction, indicating a decrease of overpotential for hydrogen evolution. Furthermore, the reduction peak and oxidation peak of Au shift cathodically and anodically, respectively, with increasing sweep rate. A linear relationship between the maximum current at peaks and the square root of sweep rate indicates that reduction and oxidation processes involving Au are diffusion-controlled.

### 3.2. Characterizations of Au NCs

Fig. 2a shows XPS spectra of ta-C, ta-C:P and ta-C:P/Au after depositing 90 s in $HAuCl_4$ solution. The peaks centered at 285.4 ± 0.2, 132.4 ± 0.2, 189.5 ± 0.2 and 533.2 ± 0.2 eV are related to C 1s, P 2p, P 2s and O 1s spectra. Au $4f_{7/2}$ and Au $4f_{5/2}$ peaks located at 83.9 ± 0.1 eV and 87.6 ± 0.1 eV for the Au NCs are consistent with those of Au foil [22]. The intensity of Au 4f peak is strengthened first and attenuated subsequently as the sputtering time (i.e. depth) increases (Fig. 2b). This hints the three-dimensional structure of Au NCs. No shift of Au 4f peak is observed, excluding the possibility of 'gold carbide' formation. The movement of C 1s peak towards lower binding energy is the result of surface graphitization after sputtering 60 s (Fig. 2c).

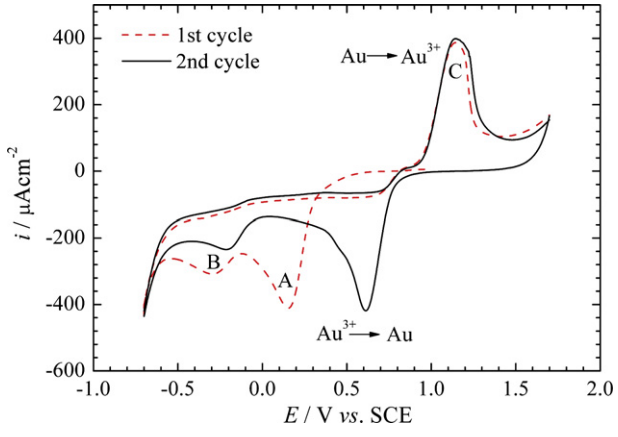


**Fig. 1.** Cycle voltammograms of ta-C:P electrode in 0.1 M $H_3BO_4 + H_2SO_4$ solution including 0.5 mM $HAuCl_4$ (pH 1.4) at 0.02 $V s^{-1}$. The apparent geometric surface area of ta-C:P is 0.4 $cm^2$.

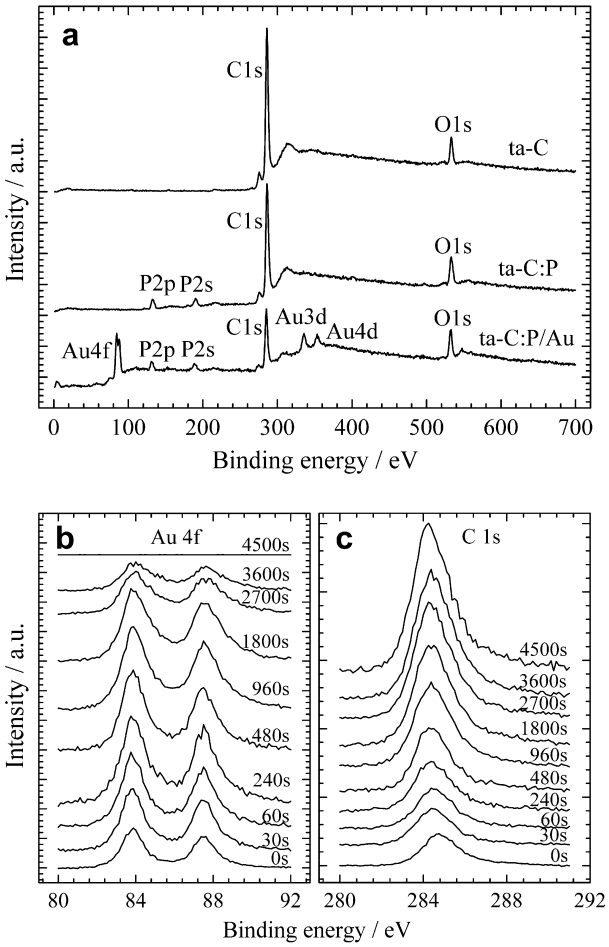


**Fig. 2.** (a) XPS spectra of ta-C, ta-C:P and ta-C:P/Au films. (b) XPS spectra of Au 4f and C 1s as a function of sputtering time for ta-C:P/Au film after depositing 90 s in $HAuCl_4$ solution.

SEM images of ta-C:P and ta-C:P/Au electrodes shown in Fig. 3 confirm the discrete nature of Au NCs on ta-C:P surface. The average number of Au NCs is predicted from SEM images and geometric working areas by image analysis software. Results show that Au NCs prepared at 20 s appear to be spherical and have a size distribution from 13.5 nm to 75.7 nm with 50.3 nm mean value (Fig. 3b). The clustering hints that the growth of some Au sites occurs around the already deposited Au seeds. When the deposition time rises up to 180 s, the average diameter of Au NCs increases to 56.9 nm with a density of $1.2 \times 10^9$ units per $cm^2$ (Table 1). The size dispersion of Au NCs becomes larger from 13.0 nm to 78.3 nm, suggesting a progressive nucleation mechanism. Chronoamperometry analysis also confirms progressive nucleation and diffusion-controlled growth of Au on ta-C:P surface using Scharifker and Hills models [23]. Similarly, increasing the deposition time to 720 s produces average 88.4 nm Au CNs with a density of $2.5 \times 10^9$ units per $cm^2$. Therefore, the deposition of Au NCs on ta-C:P surface by electrochemical method represents a growth of separate three-dimensional islands of hemispheric shape but not formation of successive monolayers.

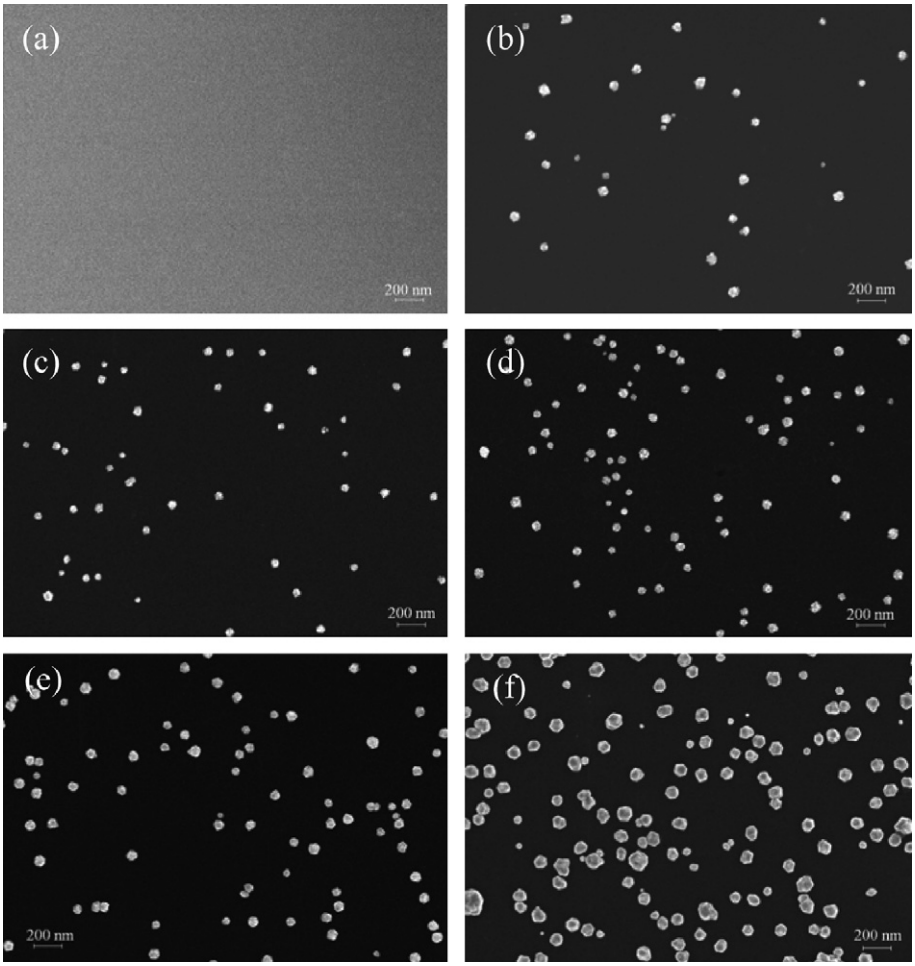


**Fig. 3.** SEM images of ta-C:P and ta-C:P/Au electrodes with different deposition times: (a) ta-C:P, (b)–(f) ta-C:P/Au for 20, 90, 180, 270 and 450 s, respectively.

**Table 1**
Parameters of ta-C, ta-C:P and ta-C:P/Au electrodes with different Au loadings obtained from SEM and voltammetry analyses

| Sample | Au deposition time (s) | Density of Au deposits (units $cm^{-2}$) | $\Delta E_p$ (mV) | $\frac{I_p^{ox}}{I_p^{red}}$ | $I_p^{ox}$ (μA) |
|---|---|---|---|---|---|
| ta-C | 0 | 0 | 510 | 0.86 | 1.8 |
| ta-C:P | 0 | 0 | 170 | 0.88 | 8.4 |
| ta-C:P/$Au_1$ | 90 | $6.6 \times 10^8$ | 87 | 0.94 | 10.5 |
| ta-C:P/$Au_2$ | 180 | $1.2 \times 10^9$ | 62 | 0.99 | 12.1 |
| ta-C:P/$Au_3$ | 270 | $1.4 \times 10^9$ | 63 | 0.98 | 13.7 |
| ta-C:P/$Au_4$ | 720 | $2.5 \times 10^9$ | 61 | 0.99 | 15.1 |

The related error for all values is less than 5%.
Aiping Liu et al.

### 3.3. Voltammetric response of ta-C:P and ta-C:P/Au electrodes

Fig. 4 displays CVs of ta-C, ta-C:P and ta-C:P/Au electrodes in 5 mM $K_3[Fe(CN)_6]$ and 1 M KCl solution. ta-C film represents slight activity to $Fe(CN)_6^{3-/4-}$ redox due to its poor conduction ($\rho = 10^7$–$10^8\ \Omega$ cm), while ta-C:P electrode ($\rho = 10$–$40\ \Omega$ cm [19]) provides a pronounced reactive signal and exhibits a non-reversible behavior with a peak potential difference ($\Delta E_p$) of 170 mV and peak current ratio ($I_p^{ox}/I_p^{red}$) of 0.88 (Table 1). Comparably, ta-C:P/Au represents an excellent reversibility towards $Fe(CN)_6^{3-/4-}$ redox and the catalytic capability is dependent on the Au loading on electrode surface. After 90 s deposition, the $\Delta E_p$ and $I_p^{ox}/I_p^{red}$ ratio of ta-C:P/$Au_1$ are equal to 87 mV and 0.94 (Table 1). These results suggest that the Au NCs on ta-C:P surface can accelerate electron exchange between ta-C:P and $Fe(CN)_6^{3-/4-}$ in the solution. The variation of repetitious measurements falls within the margin of experimental error, implying the stability of Au NCs. The $\Delta E_p$ further decreases with the increase of Au NCs loading for ta-C:P/$Au_2$ (Table 1). Subsequent increase in the deposition time does not significantly change $\Delta E_p$ and $I_p^{ox}/I_p^{red}$ ratio. Moreover, the peak current $I_p^{ox}$ on ta-C:P/Au electrodes increases 5–9 times compared with that on ta-C and 1–2 times compared with that on ta-C:P (Table 1). However, the experimental peak current on ta-C:P/Au is lower than the theoretical value calculated using the Randles–Sevcik equation [24] for a 0.4 $cm^2$ electrode area and a $7.6 \times 10^{-6}$ $cm^2\ s^{-1}$ diffusion coefficient [6]. This can be explained by the suggestion that there is a small quantity of active sites on ta-C due to the high resistivity of ta-C film. The enhanced current response on ta-C:P may be attributed to the catalyzed action of active C-P sites on ta-C:P surface [19]. Nanosized Au clusters with good conductive

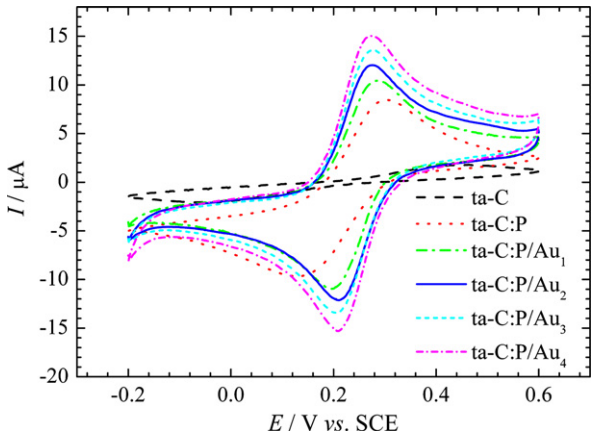


**Fig. 4.** Cyclic voltammograms of ta-C, ta-C:P and ta-C:P/Au electrodes in 5 mM $K_3[Fe(CN)_6]$ and 1 M KCl solution at 0.02 $V s^{-1}$. The apparent geometric surface areas of all electrodes are 0.4 $cm^2$.

properties further facilitate charge transfer, increase the catalytic activity and improve the reversibility of ta-C:P by adjusting the coverage and size of Au NCs. However, the active sites of ta-C:P/Au surface are still limited.

## 4. Conclusions

Three-dimensional gold nanoclusters (CNs) are deposited on phosphorus incorporated tetrahedral amorphous carbon (ta-C:P) electrode by electrodeposition. Cyclic voltammetric investigations show that Au reduction represents a three-electron, diffusion-controlled process. The size and coverage of Au NCs can be adjusted by controlling the deposition time, which dominates electrochemical properties of ta-C:P/Au electrodes. Current-time transients demonstrate that Au electrodeposition occurs as progressive nucleation at finite sites on ta-C:P, followed by a growth process limited by the diffusion. ta-C:P/Au electrodes show a high catalytic activity towards ferricyanide oxidation reaction, indicating its further potential application in electroanalysis systems.

## Acknowledgement

This work is supported by the National Natural Science Foundation of China (Grant No. 50602012).

## References

[1] Y.W.C. Cao, R.C. Jin, C.A. Mirkin, Science 297 (2002) 1536.
[2] Y. Xiao, F. Patolsky, E. Katz, J.F. Hainfeld, I. Willner, Science 299 (2003) 1877.
[3] M.C. Daniel, D. Astruc, Chem. Rev. 104 (2004) 293.
[4] C.R. Raj, T. Okajima, T. Ohsaka, J. Electroanal. Chem. 543 (2003) 127.
[5] C. Zhang, Z.Y. Zhang, B.B. Yu, J.J. Shi, X.R. Zhang, Anal. Chem. 74 (2002) 96.
[6] J. Weng, J.M. Xue, J. Wang, J.S. Ye, H.F. Cui, F.S. Sheu, Q.Q. Zhang, Adv. Funct. Mater. 15 (2005) 639.
[7] M. Chikae, K. Idegami, K. Kerman, N. Nagatani, M. Ishikawa, Y. Takamura, E. Tamiya, Electrochem. Commun. 8 (2006) 1375.
[8] Y.R. Zhang, S. Asahina, S. Yoshihara, T. Shirakashi, Electrochim. Acta 48 (2003) 741.
[9] I. Yagi, T. Ishida, K. Uosaki, Electrochem. Commun. 6 (2004) 773.
[10] E. Thune, E. Carpene, K. Sauthoff, M. Seibt, P. Reinke, J. Appl. Phys. 98 (2005) 034304.
[11] B. El Roustom, G. Foti, C. Comninellis, Electrochem. Commun. 7 (2005) 398.
[12] M.S. El-Deab, T. Okajima, T. Ohsaka, J. Electrochem. Soc. 150 (2003) A851.
[13] K.S. Yoo, B. Miller, R. Kalish, X. Shi, Electrochem. Solid-State Lett. 2 (1999) 233.
[14] A. Zeng, E. Liu, S.N. Tan, S. Zhang, J. Gao, Electroanalysis 14 (2002) 1294.
[15] R. Schnupp, R. Kuhnhold, G. Temmel, E. Burte, H. Ryssel, Biosens. Bioelectron 13 (1998) 889.
[16] Y.V. Pleskov, Y.E. Evstefeeva, A.M. Baranov, Diamond Relat. Mater. 11 (2002) 1518.
[17] N. Menegazzo, C.M. Jin, R.J. Narayan, B. Mizaikoff, Langmuir 23 (2007) 6812.
[18] A. Lagrini, C. Deslouis, H. Cachet, M. Benlahsen, S. Charvet, Electrochem. Commun. 6 (2004) 245.
[19] A.P. Liu, J.Q. Zhu, J.C. Han, H.P. Wu, W. Gao, Electroanalysis 19 (2007) 1773.
[20] S.X. Huang, H.Y. Ma, X.K. Zhang, F.F. Yong, X.L. Feng, W. Pan, X.N. Wang, Y. Wang, S.H. Chen, J. Phys. Chem. B 109 (2005) 19823.
[21] A.C. Hill, R.E. Patterson, J.P. Sefton, M.R. Columbia, Langmuir 15 (1999) 4005.
[22] L.Y. Zhao, A.C.L. Siu, J.A. Petrus, Z.H. He, K.T. Leung, J. Am. Chem. Soc. 129 (2007) 5730.
[23] B. Scharifker, G. Hills, Electrochim. Acta 28 (1983) 879.
[24] A.J. Bard, L.R. Faulkner, Electrochemical Methods: Fundamentals and Applications, Wiley, NY, 2001.